Supplemental Information for "Sudden change of the photon output field marks phase transitions in the quantum Rabi model"

Ye-Hong Chen,[1,2,3,*] Yuan Qiu,[1,2] Adam Miranowicz,[3,4] Neill Lambert,[3] Wei Qin,[3] Roberto Stassi,[3,5] Yan Xia,[1,2,†] Shi-Biao Zheng,[1,2] and Franco Nori[3,6,7,‡]

[1]*Fujian Key Laboratory of Quantum Information and Quantum Optics, Fuzhou University, Fuzhou 350116, China*
[2]*Department of Physics, Fuzhou University, Fuzhou 350116, China*
[3]*Theoretical Quantum Physics Laboratory, RIKEN Cluster for Pioneering Research, Wako-shi, Saitama 351-0198, Japan*
[4]*Institute of Spintronics and Quantum Information, Faculty of Physics, Adam Mickiewicz University, 61-614 Poznań, Poland*
[5]*Dipartimento di Scienze Matematiche e Informatiche, Scienze Fisiche e Scienze della Terra, Università di Messina, 98166, Messina, Italy*
[6]*Quantum Information Physics Theory Research Team, RIKEN Center for Quantum Computing, Wako-shi, Saitama 351-0198, Japan*
[7]*Department of Physics, University of Michigan, Ann Arbor, Michigan 48109-1040, USA*

(Dated: November 7, 2023)

Supplementary Note 1: Effective Hamiltonian for multi-photon down-conversion

The total Hamiltonian of the whole system contains two parts:

$$\begin{aligned}
H_{\rm tot} =& H_0 + H_D,\\
H_0 =& \omega a^\dagger a\left(|e\rangle\langle e| + |g\rangle\langle g| + |\mu\rangle\langle\mu|\right) + \Omega|e\rangle\langle e| + \omega_\mu|\mu\rangle\langle\mu|\\
&- g(a+a^\dagger)(|g\rangle\langle e| + |e\rangle\langle g|),\\
H_D =& \left[\Omega_p\cos(\omega_p t) + \Omega_s\cos(\omega_s t)\right]\left(|\mu\rangle\langle g| + |g\rangle\langle\mu|\right).
\end{aligned} \tag{S1}$$

The Hamiltonian H_0 can be diagonalized as

$$H_0 = \sum_{m=0}^{\infty} E_m|E_m\rangle\langle E_m| + \sum_{n=0}^{\infty}\left(\omega_\mu + n\omega\right)|\mu_n\rangle\langle\mu_n|, \tag{S2}$$

where $|E_m\rangle$ (E_m) is the mth eigenstate (eigenvalue) of the Rabi Hamiltonian H_R and $|\mu_n\rangle = |n\rangle|\mu\rangle$ is the nth eigenstate of the noninteracting term $\left(\omega_\mu|\mu\rangle\langle\mu| + \omega a^\dagger a\otimes|\mu\rangle\langle\mu|\right)$. Then, we can perform the unitary transformation

$$\begin{aligned}
H_D' =& \exp\left(iH_0 t\right)H_D\exp\left(-iH_0 t\right)\\
=& \left[\sum_{k'=p,s}\Omega_{k'}\cos(\omega_{k'}t)\right]\sum_n\sum_m\left\{c_n^{(m)}\exp\left[i(\omega_\mu+n\omega)t - iE_m t\right]|\mu_n\rangle\langle E_m| + \text{h.c.}\right\},
\end{aligned} \tag{S3}$$

where $c_n^{(m)} = \langle g|\langle n|E_m\rangle$ are probability amplitudes of the states $|n\rangle|g\rangle$ in the eigenstate $|E_m\rangle$. Then, when choosing

$$\omega_p = E_0 - \omega_\mu, \qquad \text{and} \qquad \omega_s = E_0 - \omega_\mu - 2l\omega, \qquad (l = 1,2,3\ldots) \tag{S4}$$

the Hamiltonian in Eq. (S3) can be divided into two parts: $H_D' = H_1 + H_2$, where

$$H_1 = \frac{1}{2}\left[c_0^{(0)}\Omega_p|\mu_0\rangle + c_{2l}^{(0)}\Omega_s|\mu_{2l}\rangle\right]\langle E_0| + \text{h.c.}, \tag{S5}$$

describes the resonant transitions $|\mu_0\rangle \leftrightarrow |E_0\rangle \leftrightarrow |\mu_{2l}\rangle$, and H_2 describes the off-resonance transitions. Generally, when $\Omega_{p,(s)} \ll |E_m - E_{m'}|, \omega$ ($m' \neq m$), H_2 can be effectively neglected by the rotating wave approximation because

*yehong.chen@fzu.edu.cn
†xia-208@163.com
‡fnori@riken.jp

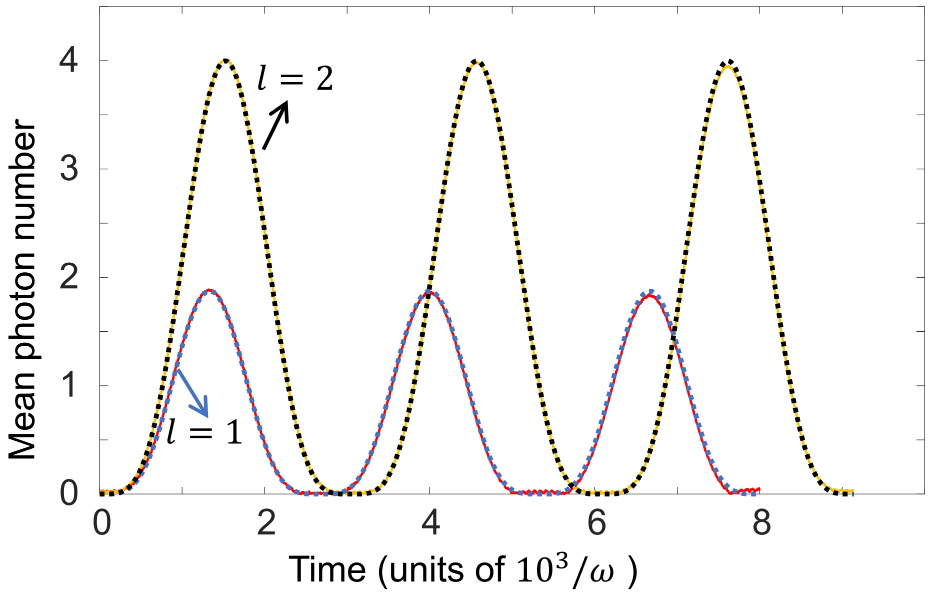

FIG. S1: **Effective and actual dynamics**. Mean photon number of the system with relatively strong drive, i.e., $\Omega_p = 0.05(E_2 - E_0)$ and $\Omega_s = 2\Omega_p$. Dotted curves: theoretical prediction according to Eqs. (16) and (17) in the main text. Solid curves: actual dynamical evolution governed by the total Hamiltonian. Other parameters are the same as those in Fig. 4 of the main text.

H_2 contains only fast-oscillating terms. However, for relatively strong driving fields such as $\Omega_{p,(s)} \gtrsim 10^{-2}\omega$, H_2 can have influence to the system dynamics, which can be estimated using second-order process [S1–S3]:

$$H_2 \approx \sum_n \sum_m \frac{|c_n^{(m)}|^2}{4} \left[\frac{|\Omega_p|^2}{E_0 - E_m + n\omega} + \frac{|\Omega_p|^2}{E_0 - E_m + n\omega - 2\omega_p} + \frac{|\Omega_s|^2}{E_0 - E_m + (n-2l)\omega} + \frac{|\Omega_s|^2}{E_0 - E_m + (n-2l)\omega - 2\omega_s} \right] (|\mu_n\rangle\langle\mu_n| - |E_m\rangle\langle E_m|) \,. \tag{S6}$$

Here, the denominators of the terms in the summation cannot be zero because it means that the corresponding transitions in Eq. (S3) are resonant when the denominators are zero.

We can assume that the influence of H_2 can be neglected by setting $\Omega_{p,(s)} \sim 10^{-3}|E_2 - E_0|$. For simplicity, we can ignore the superscript of the coefficient $c_n^{(0)}$ when considering only the eigenstate $|E_0\rangle$ in the effective dynamics. Thus, the effective Hamiltonian of Eq. (6) in the main text is obtained, i.e.,

$$H_{\rm eff} = H_1 = \frac{1}{2} \left[c_0 \Omega_p |\mu_0\rangle + c_{2l} \Omega_s |\mu_{2l}\rangle \right] \langle E_0| + \text{h.c.} \tag{S7}$$

The effective level transitions of the system described by $H_{\rm eff}$ are shown in Fig. S2(a). When the initial state for the system is $|\mu_0\rangle$, the effective level transitions in Fig. S2(a) can be understood as a multi-photon down-conversion process: The pump pulse of frequency ω_p is converted into a Stokes pulse of frequency ω_s and $2l$ cavity photons of frequency ω. At the critical point $g_c = 1$, the energy spectrum of $H_{\rm eff}$ collapses [see Fig. S2(b)] because of $c_0 \simeq c_{2l} \simeq 0$. In this case, the down-conversion process becomes invalid. It is worth noting that for relatively strong drivings, H_2 causes energy level shifts in the effective three-level system, leading to small detunings in the Raman transitions. This can affect the efficiency of the down-conversion process, e.g., leading to small oscillations (see Fig. S1) in the maximal population of the target multi-photon state $|\mu_{2l}\rangle$.

When the initial state is $|\mu_0\rangle$, the evolution of the system can be solved:

$$\begin{aligned} |\phi(t)\rangle \approx & \exp\left(-iH_{\rm eff}t\right)|\mu_0\rangle \\ = & \left[\cos(\theta)^2 + \cos(\Xi t)\sin(\theta)^2\right]|\mu_0\rangle - i\sin(\Xi t)\sin(\theta)|E_0\rangle \\ & + \frac{1}{2}\sin(2\theta)\left[\cos(\Xi t) - 1\right]|\mu_{2l}\rangle, \end{aligned} \tag{S8}$$

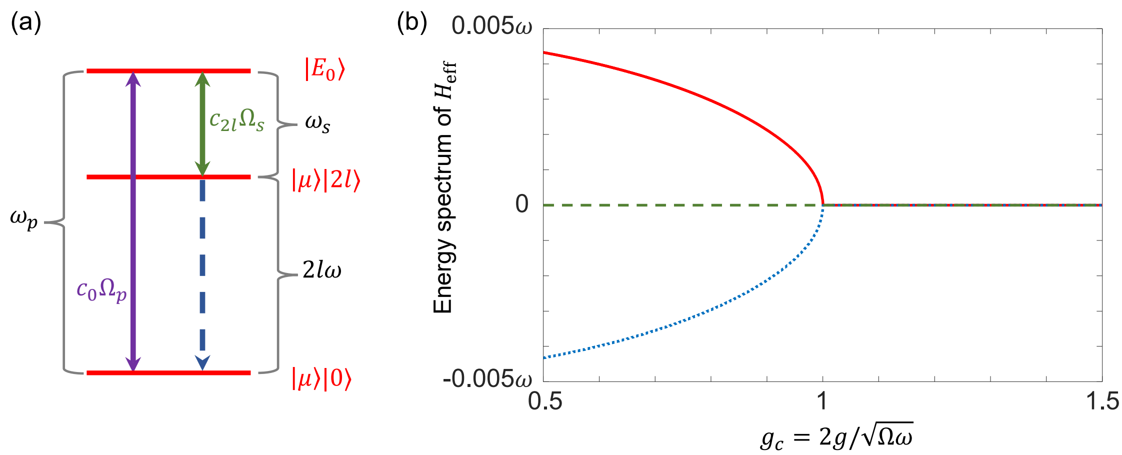

FIG. S2: **Effective model**. (a) Effective level transitions described by the effective Hamiltonian $H_{\rm eff}$. (b) Energy spectrum of the effective Hamiltonian $H_{\rm eff}$. The spectrum collapses at $g_c = 1$, which is the critical point determined by the Rabi Hamiltonian H_R. We choose $\Omega = 10^6\omega$, $\omega_\mu = E_0 - [2(n_d-4)+0.25]\,\omega$, $\Omega_p = 0.005(E_2 - E_0)$, and $\Omega_s = 2\Omega_p$ to satisfy the required conditions. Here, $n_d \geq 4$ is used to adjust the driving frequencies ω_p and ω_s. The eigenvalues E_0 and E_2 can be numerically calculated.

where

$$\Xi = \frac{1}{2}\sqrt{(c_0\Omega_p)^2 + (c_{2l}\Omega_s)^2}, \qquad \text{and} \qquad \theta = \arctan\left[c_0\Omega_p/\left(c_{2l}\Omega_s\right)\right]. \tag{S9}$$

Obviously, the population of the state $|\mu_{2l}\rangle$ reaches its maximum when $\tau = t = \pi/\Xi$. The system state at time τ becomes

$$|\phi(\tau)\rangle \approx \cos(2\theta)|\mu_0\rangle - \sin(2\theta)|\mu_{2l}\rangle = [\cos(2\theta)|0\rangle - \sin(2\theta)|2l\rangle] \otimes |\mu\rangle, \tag{S10}$$

which is a separable state. In this case, the maximum mean photon number of the system is

$$\bar{n}_{\rm max} = \langle X^- X^+\rangle|_{t=\tau} = 2l\sin(2\theta). \tag{S11}$$

Note that when the third atomic level $|\mu\rangle$ is considered, the operator X^+ should be modified as

$$X^+ = \sum_j \sum_{j'<j} \langle \xi_{j'}|a^\dagger + a)|\xi_j\rangle|\xi_{j'}\rangle\langle\xi_j|, \tag{S12}$$

where $|\xi_j\rangle$ is the jth eigenstate of H_0, i.e., $\{|\xi_j\rangle\} = \{|E_m\rangle, |\mu_n\rangle\}$.

In Fig. S3(a), we show the maximum populations

$$\mathcal{P}_{2k}^{\rm max} = \max\left[|\langle\mu_{2k}|\phi(\tau)\rangle|^2\right] \qquad (k = 0, 2), \tag{S13}$$

of the state $|\mu_{2k}\rangle$, at the time τ, versus different choices of g_c. Also, we show, in Figs. S3(b–g), the Wigner function $W(\beta)$ of the system at the time τ for different g_c. Here, the Wigner function $W(\beta)$ is defined by

$$\begin{aligned} W(\beta) =& \frac{1}{\pi}\int d^2\gamma \exp\left(\gamma^*\beta - \gamma\beta^*\right)\mathrm{Tr}[D(\gamma)|\phi(\tau)\rangle\langle\phi(\tau)|], \\ D(\gamma) =& \exp\left(\gamma a^\dagger - \gamma^* a\right), \end{aligned} \tag{S14}$$

where the atomic state can be ignored because $|\phi(\tau)\rangle$ is a separable state. As shown in Figs. S3(b–g), when the Rabi Hamiltonian is in the normal phase (i.e, $g_c < 1$), the system state at time τ is a superposition state of even Fock states. Increasing the parameter g_c results in an increase of the weight of the $2l$ Fock state $|\mu_{2l}\rangle$. When g_c approaches 1 from the left, the component of the ground state $|\mu_0\rangle$ vanishes, leaving only the $2l$ Fock state $|\mu_{2l}\rangle$. When g_c crosses the critical point, we can see a collapse of the Wigner function [see Figs. S3(f) and (g)], i.e., suddenly, the $2l$ Fock state $|\mu_{2l}\rangle$ vanishes, leaving only the ground state $|\mu_0\rangle$ in the system at the time τ. This is understood that the energy spectrum of the effective Hamiltonian $H_{\rm eff}$ collapses [see Fig. S2(b)] at the critical point of the quantum Rabi Hamiltonian.

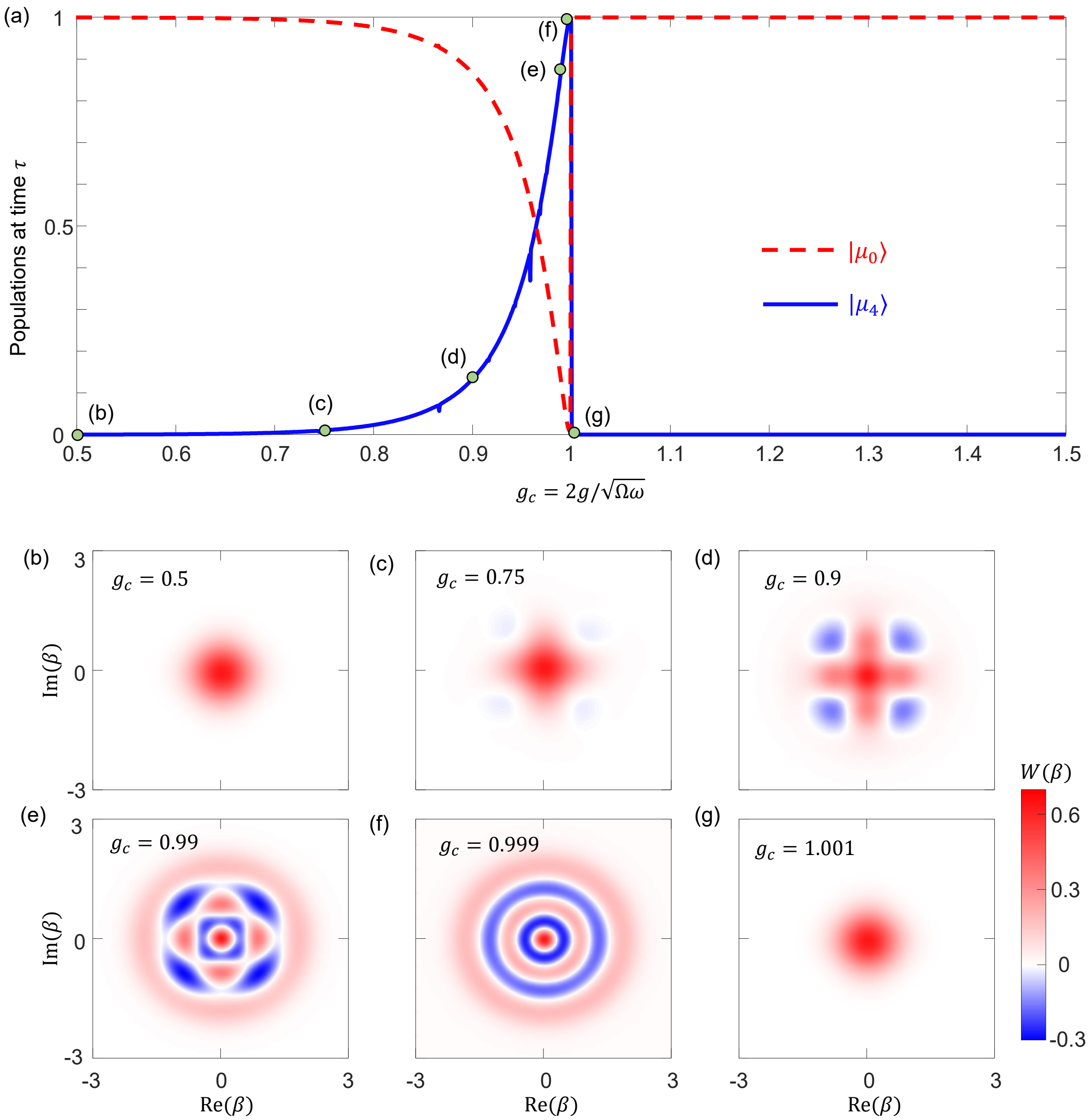

FIG. S3: **Dynamics of the model**. (a) Populations of the ground state $|\mu_0\rangle$ and the four-photon state $|\mu_4\rangle$ at the time $\tau = \pi/\Xi$ in the evolution governed by $H_{\rm tot}$ when g_c is fixed to different values. (b–g) Wigner functions $W(\beta)$ defined in Eq. (S14) for some specific values of g_c. The parameters are the same as those in Fig. S2. For $\Xi \to 0$, we impose $\Xi = 0.01\omega$ to avoid an infinite evolution time $\tau \to \infty$. The eigenvalues E_0 and E_2 can be numerically calculated. For a fixed g_c in the normal phase ($g_c < 1$), the system at the time τ is the superposition state described by Eq. (S10), while in the superradiant phase ($g_c > 1$), the system keeps in the ground state $|\mu_0\rangle$. A collapse of the Wigner function occurs at the critical point.

To indicate that a quantum phase transition occurs, the most immediate signature should be a discontinuity of the derivative of $\langle E_0|a^\dagger a|E_0\rangle$ at the critical point, i.e.,

$$\left.\frac{d\langle E_0|a^\dagger a|E_0\rangle}{dg_c}\right|_{g_c=1^-} \neq \left.\frac{d\langle E_0|a^\dagger a|E_0\rangle}{dg_c}\right|_{g_c=1^+}. \tag{S15}$$

As shown in Figs. S4(a) and S4(b), the derivative of $\langle E_0|a^\dagger a|E_0\rangle$ is discontinuous when $\Omega/\omega = 10^6$ and $\Omega/\omega = 10^4$; thus, the thermodynamic limit $\Omega/\omega \to \infty$ is effectively satisfied. For $\Omega/\omega = 10^2$, the phenomenon becomes less pronounced [see Fig. S4(c)]. For comparision, we show the Fig. 4(a) of the main text (here as Fig. S5) displaying the

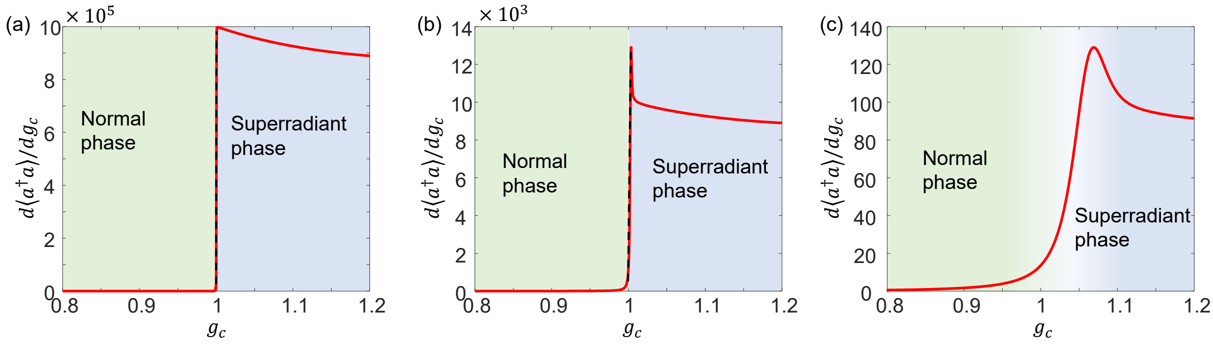

FIG. S4: **Phase transition**. Derivative of $\langle E_0|a^\dagger a|E_0\rangle$ (i.e., the virtual cavity excitation number) in the ground eigenstate of the quantum Rabi model when (a) $\Omega/\omega = 10^6$, (b) $\Omega/\omega = 10^4$, and (c) $\Omega/\omega = 10^2$. For (a) and (b), the derivative curves are discontinuous at $g_c = 1$ indicating the occurrence of the quantum phase transition. For (c), the transition of two different phases is smooth.

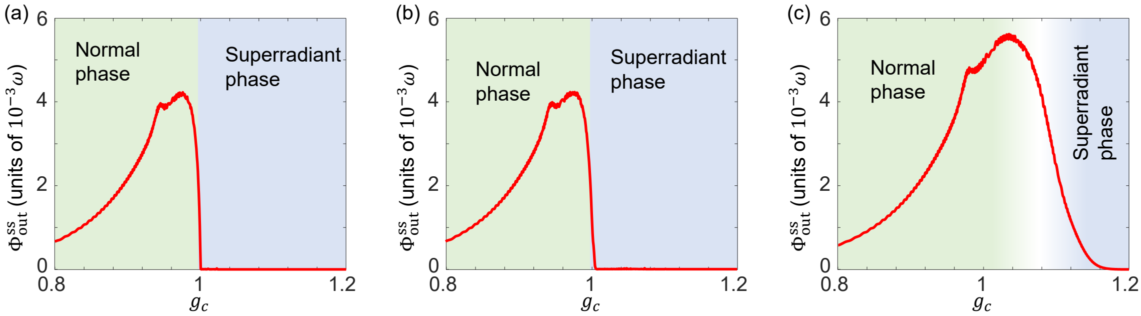

FIG. S5: **Photon output rate**. Steady-state output photon rates $\Phi_{\rm out}^{\rm ss} = \Phi_{\rm out}|_{t\to\infty}$ given in our protocol when (a) $\Omega/\omega = 10^6$, (b) $\Omega/\omega = 10^4$, and (c) $\Omega/\omega = 10^2$. For (a) and (b), the output photon rates are discontinuous at $g_c = 1$, which coincide very well with the curves in Figs. S4(a) and S4(b), respectively. For (c), the transition of two different phases is smooth.

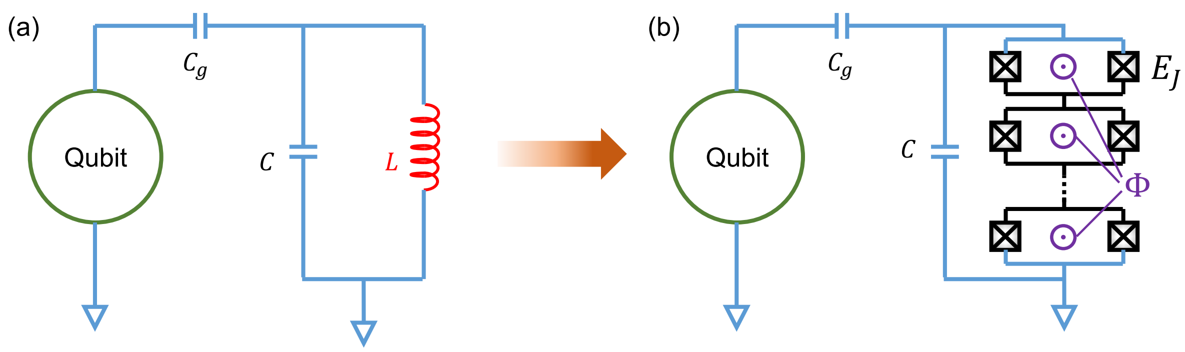

FIG. S6: **Schematic representation**. A qubit (green) couples to (a) an LC resonator, (b) an array of dc SQUIDS.

steady-state output field of the system for different frequency rates. At the critical point, the output photon field of the system changes abruptly (see Fig. S5), which coincides very well with the change of $\langle E_0|a^\dagger a|E_0\rangle$ (see Fig. S4). This gives a signature for the occurrence of the quantum phase transition.

Supplementary Note 2: Possible implementations using superconducting quantum circuits

The past decade has seen a rapid increase in light-matter couplings [S10–S12]. Some experimental observations of the ultrastrong light-matter coupling in superconducting quantum circuits are listed in Table S1. Generally, the circuits in the experiments [S4–S9] can be simplified as an artificial atom coupled with an LC resonator [see Fig. S6(a)] via a capacitance.

To realize the atomic three-level construction, we need a relatively strong anharmonicity for the artificial atom, so that the third level (as well as other levels) is far off-resonance to the resonator frequency. For this goal, we can use an artificial atom which is constituted by three junctions in the superconducting circuit, i.e., a flux qubit. Assuming that two larger junctions have equal Josephson energies $E_J = E_{J1} = E_{J2}$ and capacitances $C_J = C_{J1} = C_{J2}$, while for the third junction $E_{J3} = \alpha E_J$ and $C_{J3} = \alpha C_J$, with $\alpha < 1$. The Hamiltonian of the artificial atom is

$$H_a = \frac{P_p^2}{2M_p} + \frac{P_m^2}{2M_m} + U(\varphi_p, \varphi_m), \tag{S16}$$

where $P_p = -i\hbar\partial/\partial\varphi_p$, $P_m = -i\hbar\partial/\partial\varphi_m$, $M_p = 2C_J(\phi_0/2\pi)^2$, and $M_m = M_p(1+2\alpha)$. Here, $\varphi_p = (\varphi_1 + \varphi_2)/2$ and $\varphi_m = (\varphi_1 - \varphi_2)/2$ are defined by the phase drops φ_1 and φ_2 across the two larger junctions. In addition, $\phi_0 = \hbar/(2e)$ is the superconducting flux quantum. The effective potential is

$$U(\varphi_p, \varphi_m) = 2E_J(1 - \cos\varphi_p \cos\varphi_m) + \alpha E_J[1 - \cos(2\pi f + 2\varphi_m)], \tag{S17}$$

where $f = \phi_e/\phi_0$ is the reduced magnetic flux. It is clear that the shape of the double-well potential energy $U(\varphi_p, \varphi_m)$ can be changed from asymmetric to symmetric if f is changed from $f \neq 0.5$ to $f = 0.5$ by adjusting the external magnetic flux ϕ_e. Thus, ϕ_e is a control parameter for various properties of these flux-qubit circuits.

The desired transition energies of our protocol can be obtaining at $f \simeq 0.53$. By using $E_J = 6500$ GHz, $E_C = 180$ GHz and $\alpha = 0.8$, one can obtain

$$\begin{aligned} \omega_1 - \omega_0 &\simeq 2\pi \times 250 \text{ GHz}, \\ \omega_2 - \omega_1 &\simeq 2\pi \times 50 \text{ GHz}, \\ \omega_3 - \omega_2 &\simeq 2\pi \times 75 \text{ GHz}. \end{aligned} \tag{S18}$$

The anharmonicity of the artificial atom is strong enough to decouple the ground state to the cavity.

Then, by applying a flux drive to the artificial atom, the control Hamiltonian becomes

$$H_C = [\Omega_p \cos(\omega_p t) + \Omega_s \cos(\omega_s t)] \sum_n \left(|n\rangle\langle n+1| + |n+1\rangle\langle n|\right), \tag{S19}$$

where $|n\rangle$ is the nth level of the artificial atom. Because ω_p and ω_s are very close to the transition frequency $\omega_1 - \omega_0$, the flux drive can only induce transitions between the ground and the first-excited states of the artificial atom, while the other level transitions are far off resonance driven.

The Hamiltonian of the LC resonator is given by

$$H_{LC} = 4E_C\hat{q}^2 + \frac{E_L}{2}\hat{\varphi}^2, \tag{S20}$$

where $E_C = e^2/(2C)$ and $E_L = 1/(4e^2L)$. The dimensionless charge and flux operators $\hat{q}$ and $\hat{\varphi}$ obey the commutation relations $[\hat{\varphi}, \hat{q}] = i$. Following the standard quantization procedure for circuits

$$\hat{\varphi} = \left(\frac{2E_C}{E_L}\right)^{\frac{1}{4}} \left(a^\dagger + a\right), \qquad \text{and} \qquad \hat{q} = i\left(\frac{E_L}{32E_C}\right)^{\frac{1}{4}} \left(a^\dagger - a\right), \tag{S21}$$

TABLE S1: Superconducting experiments that have achieved the ultrastrong light-matter coupling. Abbreviations are FQ=flux qubit, TR=transmon qubit, TL=transmission line resonator, and LE=lumped-element resonator.

Year & Ref.	Qubit	Cavity	$g/2\pi$ (MHz)	$\omega/2\pi$ (GHz)	g/ω
2010 [S4]	FQ	TL	636	5.357	0.12
2010 [S5]	FQ	LE	810	8.13	0.1
2017 [S6]	FQ	LE	7630	5.711	1.34
2017 [S7]	FQ	LE	5310	6.203	0.86
2017 [S8]	TR	TL	897	4.268	0.19
2018 [S9]	FQ	LE	7480	6.335	1.18

we can diagonalize the Hamiltonian H_{LC} as

$$H_{LC} = \omega \left(a^\dagger a + \frac{1}{2} \right), \tag{S22}$$

where $\omega = \sqrt{8E_C E_L} = 1/\sqrt{LC}$. In this case, in order to reduce the cavity frequency ω to satisfy the $\Omega/\omega \to \infty$ limit, one needs to choose a very large C and L, which could be difficult in current experiments.

To overcome this problem, we suggest using an array of dc superconducting quantum interference devices (SQUIDs) to replace the LC resonator, as shown in Fig. S6(b). The Hamiltonian of this array of Cooper pairs reads

$$H_A = 4E_C \hat{n}^2 - N_0 E_J(\Phi) \cos \left(\frac{\hat{\varphi}}{N_0} \right). \tag{S23}$$

Here, $\hat{n}$ and $\hat{\varphi}$ satisfying $[\hat{\varphi}, \hat{n}] = i$ are the number of Cooper pairs and the overall phase across the junction array, respectively; $E_J(\Phi)$ is the Josephson energy of a single SQUID, which can be adjusted by the external-magnetic flux Φ; and N_0 is the total number of the SQUID in the array. For $N_0 \gg \hat{\varphi}$, H_A can be simplified as

$$H_A \approx 4E_C \hat{n}^2 - N_0 E_J(\Phi) \left[1 - \frac{1}{2} \left(\frac{\hat{\varphi}}{N_0} \right)^2 \right] = 4E_C \hat{n}^2 + \frac{E_J(\Phi)}{2N_0} \hat{\varphi}^2 - N_0 E_J(\Phi), \tag{S24}$$

Using the quantization procedure

$$\hat{\varphi} = \left[\frac{N_0 E_C}{E_J(\Phi)} \right]^{\frac{1}{4}} \left(a^\dagger + a \right), \qquad \text{and} \qquad \hat{n} = i \left[\frac{E_J(\Phi)}{32 N_0 E_C} \right]^{\frac{1}{4}} \left(a^\dagger - a \right), \tag{S25}$$

the Hamiltonian H_A is diagonalized as

$$H_A \approx \omega \left(a^\dagger a + \frac{1}{2} \right) - N_0 E_J(\Phi), \tag{S26}$$

where the cavity frequency

$$\omega = \sqrt{\frac{8E_C E_J(\Phi)}{N_0}}, \tag{S27}$$

is adjustable with the parameters Φ and N_0. This allows us to reduce the frequency ω to reach the $\Omega/\omega > 10^3$ limit and the critical point $g_c = 1$. For instance, we can choose

$$E_C = 2\pi \times 100 \text{ MHz}, \qquad E_J(\Phi) = E_C/8 = 2\pi \times 12.5 \text{ MHz}, \qquad N_0 = 400, \tag{S28}$$

so that $\omega = 2\pi \times 5$ MHz. The qubit frequency can be chosen as $\Omega \sim 2\pi \times 50$ GHz, which could be possible using, e.g., flux qubits [S10, S11, S13–S15]. These allow to reach $\Omega/\omega = 10^4$. In this case, the coupling strength to reach the critical point $g_c = 1$ is $g = 50\omega \simeq 2\pi \times 250$ MHz.

Supplementary Note 3: Quantum phase transition in a simulated quantum Rabi model

Another possible way to verify our proposal is using a simulated quantum Rabi model [S16–S19]. Here, we present a possible implementation of our method in a simulated quantum Rabi model induced by a squeezing-light field [S16, S17]. Assuming that the three-level atom weakly couples to a cavity with coupling strength η, the system can be described by the Jaynes-Cummings Hamiltonian under the rotating-wave approximation:

$$H_{\text{JC}} = \omega_b b^\dagger b + \omega_e |e\rangle\langle e| + \omega_\mu |\mu\rangle\langle\mu| - \eta (b^\dagger |g\rangle\langle e| + b|e\rangle\langle g|), \tag{S29}$$

where ω_b is the bare frequency of the cavity b and ω_e is the level frequency of the state $|e\rangle$. The cavity is subjected to a two-photon (i.e. parametric) drive with amplitude Ω_{nl} and frequency ω_{nl}:

$$H_{\text{nl}} = -\frac{\Omega_{\text{nl}}}{2} \left[b^{\dagger 2} \exp(-i\omega_{\text{nl}} t) + b^2 \exp(i\omega_{\text{nl}} t) \right]. \tag{S30}$$

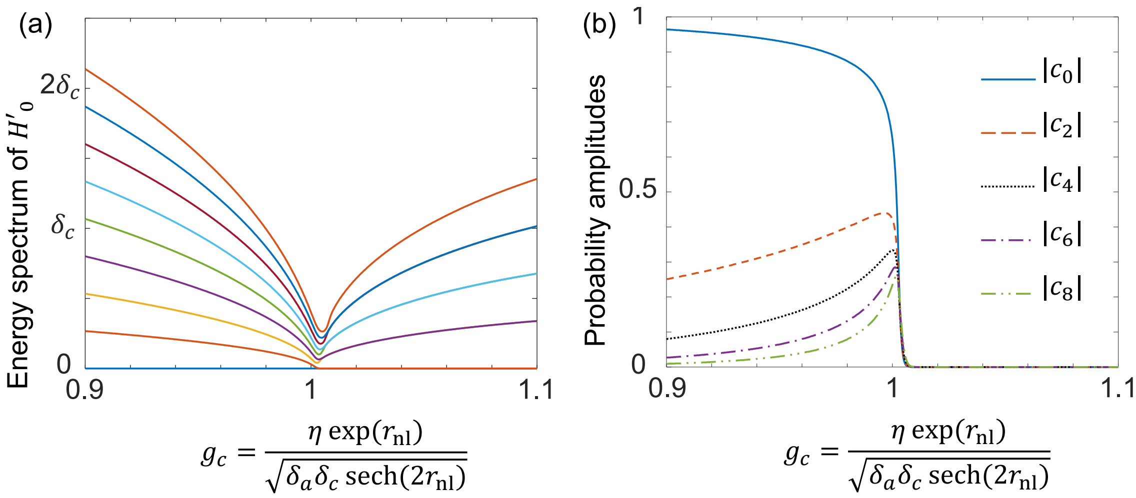

FIG. S7: **Energy spectrum and probability amplitudes**. (a) Energy spectrum of the anisotropic Rabi Hamiltonian H_0' in Eq. (S33), where g_c is defined in Eq. (S35). We impose the eigenvalue of the ground eigenstate to be 0. (b) Probability amplitudes $|c_{2k}| = \langle g|\langle 2k|S^\dagger(r_{\rm nl})S(r_{\rm nl})|E_0\rangle$ of the states $S(r_{\rm nl})|2k\rangle|g\rangle$ in the ground eigenstate of H_0' in Eq. (S33) calculated for different g_c. We choose parameters $r_{\rm nl} = 0.5$ and $\delta_a = 10^4\delta_c{\rm sech}(2r_{\rm nl}) \approx 6.841\times 10^3\delta_c$, which correspond to the frequency ratio $\Omega/\omega = 10^4$. With there parameters, the collapse of the energy spectrum is shifted to $g_c \simeq 1.002$ due to the finite-frequency effect.

Then, working in a frame rotating at half of the parametric drive frequency $\omega_{\rm nl}/2$, the system Hamiltonian becomes:

$$\begin{aligned} H_0' = H_{\rm JC} + H_{\rm nl} =& \delta_c b^\dagger b + \delta_a|e\rangle\langle e| + \omega_\mu|\mu\rangle\langle\mu| \\ &- \frac{\Omega_{\rm nl}}{2}\left(b^{\dagger 2} + b^2\right) - \eta(b^\dagger|g\rangle\langle e| + b|e\rangle\langle g|), \end{aligned} \tag{S31}$$

where $\delta_c = \omega_b - \omega_{\rm nl}/2$ and $\delta_a = \omega_e - \omega_{\rm nl}/2$ are detunings. Upon introducing the Bogoliubov squeezing transformation

$$b_s = S^\dagger(r_{\rm nl})bS(r_{\rm nl}) = \cosh(r_{\rm nl})b - \sinh(r_{\rm nl})b^\dagger, \tag{S32}$$

the Hamiltonian H_0' in Eq. (S31) becomes

$$\begin{aligned} H_0' =& \delta_c{\rm sech}(2r_{\rm nl})b_s^\dagger b_s + \delta_a|e\rangle\langle e| + \omega_\mu|\mu\rangle\langle\mu| \\ &- \left[\eta\cosh(r_{\rm nl})b_s + \eta\sinh(r_{\rm nl})b_s^\dagger\right]|e\rangle\langle g| \\ &- \left[\eta\cosh(r_{\rm nl})b_s + \eta\sinh(r_{\rm nl})b_s^\dagger\right]|g\rangle\langle e|, \end{aligned} \tag{S33}$$

where

$$r_{\rm nl} = \frac{1}{4}\ln\left(\frac{\delta_c + \Omega_{\rm nl}}{\delta_c - \Omega_{\rm nl}}\right). \tag{S34}$$

Note that b_s and $b_s^\dagger$ satisfy $[b_s, b_s^\dagger] = 1$, i.e., b_s is also a bosonic mode. For this bosonic mode, the ground state is the squeezed vacuum state $S(r_{\rm nl})|0\rangle_b$, where the state $|n=0\rangle_b$ is the vacuum state of the cavity mode b. The Hamiltonian H_0' describes the anisotropic Rabi model, which can also exhibit a superradiant quantum phase transition in the $\delta_a/\left[\delta_c{\rm sech}(2r_{\rm nl})\right] \to \infty$ limit [S20]. The critical point for H_0' is at

$$g_c = \frac{\eta\cosh(r_{\rm nl}) + \eta\sinh(r_{\rm nl})}{\sqrt{\delta_a\delta_c{\rm sech}(2r_{\rm nl})}} = \frac{\eta\exp(r_{\rm nl})}{\sqrt{\delta_a\delta_c{\rm sech}(2r_{\rm nl})}} = 1. \tag{S35}$$

That is, the quantum phase transition exhibited by this anisotropic Rabi Hamiltonian is the same as that exhibited by the standard quantum Rabi Hamiltonian [S20]:

$$H_R' \simeq \delta_c{\rm sech}(2r_{\rm nl})b_s^\dagger b_s + \delta_a|e\rangle\langle e| + \omega_\mu|\mu\rangle\langle\mu| - \frac{\eta}{2}\exp(r_{\rm nl})(b_s + b_s^\dagger)(|g\rangle\langle e| + |e\rangle\langle g|). \tag{S36}$$

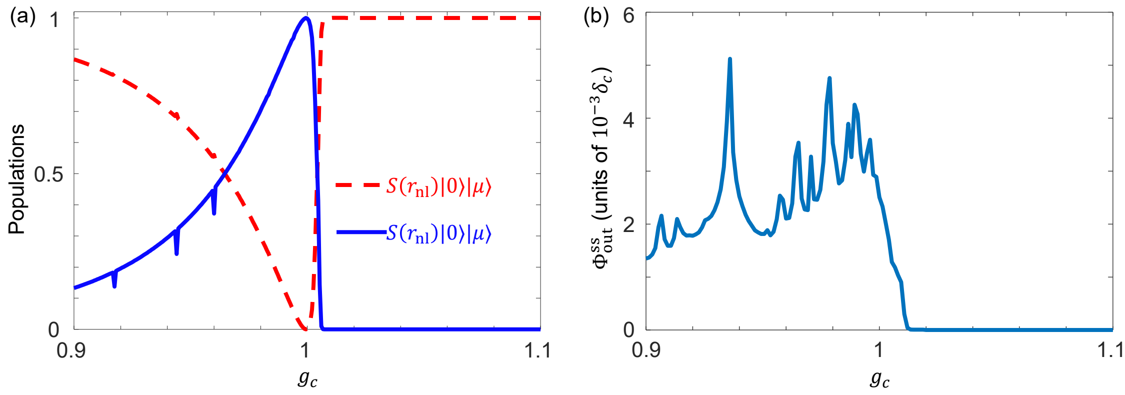

FIG. S8: **Phase transition in a simulated quantum Rabi model**. (a) Populations of the squeezed-vacuum state $S(r_{\rm nl})|0\rangle|\mu\rangle$ and the squeezed-four-photon state $S(r_{\rm nl})|4\rangle|\mu\rangle$ at the time $\tau = \pi/\Xi$ in the evolution governed by $H'_{\rm tot}$ when g_c is fixed to different values. We choose driving amplitudes $\Omega_p = 0.005(E_2 - E_0)$ and $\Omega_s = 2\Omega_p$. (b) Steady-state output rate $\Phi_{\rm out}^{\rm ss}$ defined in Eq. (S43). We choose relatively strong driving fields, i.e., $\Omega_p = 0.05(E_2 - E_0)$ and $\Omega_s = 2\Omega_p$, to achieve relatively large output photon rates. Strong driving fields may cause small errors (via counter-rotating effects) in obtaining the effective Hamiltonian $H_{\rm eff}$, leading to oscillations in $\Phi_{\rm out}^{\rm ss}$ in the normal phase, i.e., $g_c < 1$. The dissipation rates are $\kappa = \gamma_1 = \gamma_2 = 10^{-3}\delta_c {\rm sech}(2r_{\rm nl})$. Other parameters are the same as those in Fig. S7.

Figure S7(a) shows the energy spectrum of the anistropic Rabi Hamiltonian H'_0. We can see that the energy spectrum nearly collapses when $g_c \simeq 1$. Meanwhile, the probability amplitudes of different photonic-state components

$$|c_{2k}| = \langle g|\langle 2k|S^\dagger(r_{\rm nl})S(r_{\rm nl})|E_0\rangle, \tag{S37}$$

also collapse, as shown in Fig. S7(b). These indicate that the quantum phase transition exhibited by the anisotropic Rabi Hamiltonian in Eq. (S33) is the same as that exhibited by the standard quantum Rabi Hamiltonian.

For simplicity, we can choose the parameters

$$\omega = \delta_c {\rm sech}(2r_{\rm nl}), \qquad \Omega = \delta_a, \qquad g = \frac{\eta}{2}\exp(r_{\rm nl}), \qquad a = b_s, \tag{S38}$$

so that $H_0 = H_R = H'_R$, where H_0 is given in Eq. (S1). Therefore, by driving the atomic transition $|g\rangle \leftrightarrow |\mu\rangle$ with the Hamiltonian H_D in Eq. (S1), the system dynamics is the same as that discussed in Appendix A. The difference is that the Fock state $|n\rangle$ discussed in Appendix A should be replaced with the squeezed Fock state $S(r_{\rm nl})|n\rangle_b$. The total Hamiltonian for the system in the lab frame becomes

$$H'_{\rm tot} = H_{\rm JC} + H_{\rm nl} + H_D. \tag{S39}$$

For simplicity, in the following discussions we ignore the subscript b for the cavity mode, i.e., $|n\rangle_b$ is simplified to $|n\rangle$. According to the derivation in Appendix A, the evolution governed by Eq. (S39) is

$$\begin{aligned}|\phi'(t)\rangle \approx& \left[\cos(\theta)^2 + \cos(\Xi t)\sin(\theta)^2\right] S(r_{\rm nl})|\mu_0\rangle - i\sin(\Xi t)\sin(\theta)S(r_{\rm nl})|E_0\rangle \\ &+ \frac{1}{2}\sin(2\theta)\left[\cos(\Xi t) - 1\right] S(r_{\rm nl})|\mu_{2l}\rangle,\end{aligned} \tag{S40}$$

where the parameters are defined in Appendix A. Choosing possible experimental parameters:

$$r_{\rm nl} = 0.5, \qquad \delta_c/2\pi = 1 \text{ MHz}, \qquad \delta_a/2\pi \simeq 6.841 \text{ GHz}, \tag{S41}$$

and the initial state $S(r_{\rm np})|0\rangle|\mu\rangle$, for different g_c, the populations for the states $S(r_{\rm nl})|0\rangle|\mu\rangle$ and $S(r_{\rm nl})|4\rangle|\mu\rangle$ at the time τ are shown in Fig. S8(a). Similar to Fig. S3(a), we can find a sudden change of these populations near the critical point in Fig. S8(a), indicating a sudden change of the photon number distributions.

Note that the system governed by the Hamiltonian $H'_{\rm tot}$ contains only real cavity photons. We can use the standard input-output theory to study the output cavity photon rate. The master equation for this system is

$$\rho = i\left[\rho, H'_{\rm tot}\right] + \kappa\mathcal{D}[b] + \gamma_1\mathcal{D}[|g\rangle\langle e|] + \gamma_2\mathcal{D}[|\mu\rangle\langle g|], \tag{S42}$$

where κ is the decay rate of the cavity mode b and $\gamma_{1,(2)}$ is the spontaneous emission rate of the transition $|g\rangle \to |\mu\rangle$ ($|e\rangle \to |g\rangle$). The steady-state output photon rates, defined by

$$\Phi_{\rm out}^{\rm ss} = \Phi_{\rm out}|_{t\to\infty} = \kappa {\rm Tr}\left[b^{\dagger} b \rho(t\to\infty)\right], \tag{S43}$$

are shown in Fig. S8(b). We can find that the output photon rate $\Phi_{\rm out}^{\rm ss}$ suddenly vanishes when g_c is tuned across the critical point. This phenomenon is the same as that discussed for the standard quantum Rabi model in the main text. It is worth noting that relatively strong drivings chosen for Fig. S8(b) induce counter-rotating effects. These may excite the system to the higher levels of H_R' at some specific values of g_c, leading to the increase of $\Phi_{\rm out}^{\rm ss}$ at those values.

Supplementary Reference

[S1] G. S. Agarwal, *Quantum Optics* (Cambridge University Press, Cambridge, England, 2012).
[S2] M. O. Scully and M. S. Zubairy, *Quantum Optics* (Cambridge University Press, Cambridge, England, 1997).
[S3] D. F. James and J. Jerke, Can. J. Phys. **85**, 625 (2007).
[S4] T. Niemczyk, F. Deppe, H. Huebl, E. P. Menzel, F. Hocke, M. J. Schwarz, J. J. Garcia-Ripoll, D. Zueco, T. Hümmer, E. Solano, et al., Nat. Phys. **6**, 772 (2010).
[S5] P. Forn-Díaz, J. Lisenfeld, D. Marcos, J. J. García-Ripoll, E. Solano, C. J. P. M. Harmans, and J. E. Mooij, Phys. Rev. Lett. **105**, 237001 (2010).
[S6] F. Yoshihara, T. Fuse, S. Ashhab, K. Kakuyanagi, S. Saito, and K. Semba, Nat. Phys. **13**, 44 (2016).
[S7] F. Yoshihara, T. Fuse, S. Ashhab, K. Kakuyanagi, S. Saito, and K. Semba, Phys. Rev. A **95**, 053824 (2017).
[S8] S. J. Bosman, M. F. Gely, V. Singh, A. Bruno, D. Bothner, and G. A. Steele, npj Quant. Info. **3** (2017).
[S9] F. Yoshihara, T. Fuse, Z. Ao, S. Ashhab, K. Kakuyanagi, S. Saito, T. Aoki, K. Koshino, and K. Semba, Phys. Rev. Lett. **120**, 183601 (2018).
[S10] X. Gu et al., Phys. Rep. **718-719**, 1 (2017).
[S11] A. F. Kockum, A. Miranowicz, S. D. Liberato, S. Savasta, and F. Nori, Nat. Rev. Phys. **1**, 19 (2019).
[S12] P. Forn-Díaz, L. Lamata, E. Rico, J. Kono, and E. Solano, Rev. Mod. Phys. **91**, 025005 (2019).
[S13] P. Krantz, M. Kjaergaard, F. Yan, T. P. Orlando, S. Gustavsson, and W. D. Oliver, Appl. Phys. Rev. **6**, 021318 (2019).
[S14] M. Kjaergaard, M. E. Schwartz, J. Braumüller, P. Krantz, J. I.-J. Wang, S. Gustavsson, and W. D. Oliver, Ann. Rev. Cond. Mat. Phys. **11**, 369 (2020).
[S15] S. Kwon, A. Tomonaga, G. L. Bhai, S. J. Devitt, and J.-S. Tsai, J. Appl. Phys. **129**, 041102 (2021).
[S16] W. Qin et al., Phys. Rev. Lett. **120**, 093601 (2018).
[S17] C. Leroux, L. C. G. Govia, and A. A. Clerk, Phys. Rev. Lett. **120**, 093602 (2018).
[S18] C. Sánchez Muñoz et al., Phys. Rev. A **102**, 033716 (2020).
[S19] Y.-H. Chen et al., Phys. Rev. Lett. **126**, 023602 (2021).
[S20] L.-T. Shen, Z.-B. Yang, H.-Z. Wu, and S.-B. Zheng, Phys. Rev. A **95**, 013819 (2017).